Robotic Modular Leg: Design, Analysis, and Experimentation

Wael Saab

Robotics and Mechatronics Laboratory,
Mechanical Engineering,
Virginia Tech,
Blacksburg, VA 24061
e-mail: waelsaab@vt.edu

William S. Rone

Robotics and Mechatronics Laboratory,
Mechanical Engineering,
Virginia Tech,
Blacksburg, VA 24061
e-mail: wsrone@vt.edu

Pinhas Ben-Tzvi

Robotics and Mechatronics Laboratory,
Mechanical Engineering,
Virginia Tech,
Blacksburg, VA 24061;
Electrical and Computer Engineering,
Virginia Tech,
Blacksburg, VA 24061
e-mail: bentzvi@vt.edu

This paper presents the design and analysis of a reduced degree-of-freedom (DOF) robotic modular leg (RML) mechanism. The RML is composed of a two serially connected four-bar mechanisms that utilize mechanical constraints between articulations to maintain a parallel orientation between the foot and body without the use of an actuated ankle. Kinematic and dynamic models are developed for the leg mechanism and used to analyze actuation requirements and aid motor selection. Experimental results of an integrated prototype tracking a desired foot trajectory are analyzed to improve the accuracy and repeatability of the mechanism. The prototype weighs 4.7 kg and measures 368 mm in a fully extended configuration and exhibits a maximum deviation from the straight line support phase equivalent to 5.2 mm.
[DOI: 10.1115/1.4035685]

1 Introduction

In recent years, there has been a surge of research conducted in the field of multilegged robotics due to the high adaptability of legged locomotion on unstructured terrain [1–3]. Conventional multilegged robotic designs consist of a large number of active degrees-of-freedom (DOFs) that enhance locomotion and tasking abilities; however, each additional DOF increases the robot's weight, energy consumption, and complexity of trajectory planning and control [4,5]. Therefore, if a leg mechanism can be designed with reduced-DOFs at the cost of reduced articulation, while achieving similar walking functionalities, multilegged platforms may be constructed with less weight, reduced cost, and simplified controllers [6].

The majority of multilegged robots are bio-inspired from animals that have evolved over the years to adapt to their natural habitats. These robots utilize multi-DOF leg mechanisms to position their (primarily) single point of contact feet to walk and steer

on both flat and uneven terrain. Therefore, a 2n-legged robot requires 6n actuators, where n is the number of leg pairs [7]. If flat feet are implemented into the leg mechanism to enhance stability and disturbance rejection capabilities [8], additional DOFs are required to control foot orientation during a walking gait.

To address these issues, researchers have investigated methods to reduce the number of actuated joints in multilegged robotic systems. Torige et al. [9] developed a six-segment centipedelike walking robot with four motors per segment. In this design, point contact was sufficient to provide a stable support polygon since at least 3 ft was in contact with the ground during the demonstrated walking gait. Therefore, a 2n-legged robot utilized 4n active joints. Similarly, Hoffman and Wood [10] designed a microscale centipede robot with passive revolute joints located between repeated two-legged segments. For each segment, the two legs were passively coupled to two linear actuators that provide opposing moments about the center-of-mass (COM), causing the body to extend, raise the legs, and propel robot forward. In this design, the 2n-legged robot utilized 2n active joints. The RHex hexapod robot, a six legged robot, was designed with six actuated DOFs that continuously rotate compliant C-shaped legs that propel the robot forward with steering provided by differential drive [11]. A similar design concept utilizing continuous rotation legs was implemented on a centipede robot with an additional active DOF incorporated between body segments [12]. Yoenda et al. [13] designed a quadruped robot with four active DOF. The quadruped robot, capable of performing a creeping gait, was separated into front and rear sections connected using an active revolute joint capable of rolling in the horizontal direction. The roll of the body coupled with rotation of U-shaped front and rear legs with point contact feet caused the robot to move forward. There has also been considerable amounts of research in 1DOF crank-driven mechanisms [14–18], 2DOF leg designs [19,20] that approximate straight line foot paths similar to the Jansen mechanism path curve, and passive dynamic walkers [21] that utilize less control and energy in comparison to powered robots.

This paper presents the design, analysis, and experimentation of a reduced-DOF robotic modular leg (RML) mechanism. The long term goal of this research is to develop planar walking robots, constructed by interconnecting multiple RMLs [22], to investigate the performance improvements that attached robotic tails can provide in terms of stabilization and maneuverability [22–30].

This paper is organized as follows: Section 2 presents the mechanical design concept of the RML. Section 3 presents the kinematic and dynamic models of the RML. Section 4 presents the foot trajectory planning. Section 5 presents the results associated with the actuation analysis using the RML model and the experimental results of an integrated RML prototype tracking a foot trajectory to improve the mechanism's accuracy and repeatability. Concluding remarks and future work are discussed in Sec. 6.

2 Mechanical Design

This section presents the mechanical design of the RML and the method used to build a quadruped and biped robot. Figure 1 shows a side view of the RML. The RML is a 2DOF mechanism composed of two serially connected four-bar mechanisms analogous to a thigh and shin. The thigh rotates at the hip joints, and the shin rotates at the knee joints. The two four-bar mechanism dimensions are designed to be parallelograms, which results in double-rocker behavior. Therefore, the knee and foot links remain parallel to the body as the thigh and shin links move. This method kinematically maintains a flat foot orientation without the use of an additional actuator at the ankle. On flat surfaces, planar feet provide a more stable support polygon in comparison to feet with a single point or line contact [8].

As seen in Fig. 1, the thigh is actuated directly by a hip motor mounted within the body link, while the shin is actuated by a thigh-mounted motor. A timing belt system transmits the thigh-
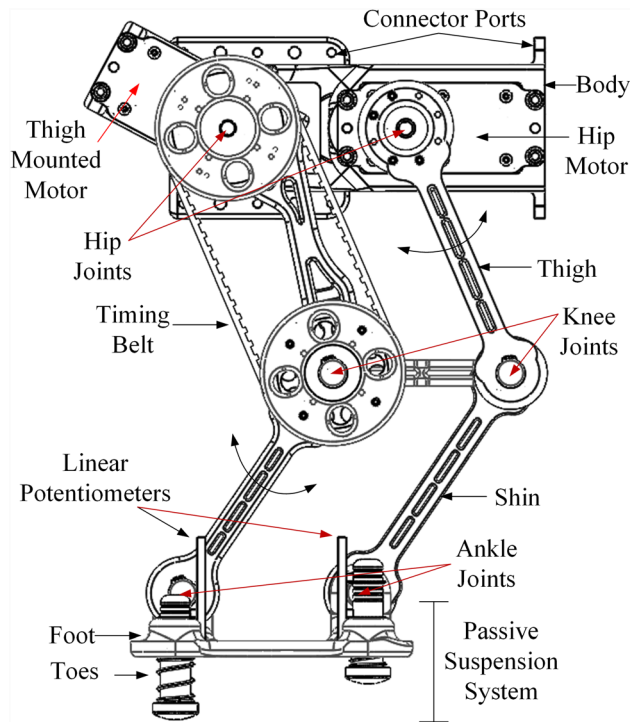
Fig. 1   Side view schematic diagram of the RML

mounted motor actuation to the shin link at the knee joint. This motor configuration controls the relative motion of these links without the need for input compensation for the hip motor. In addition, this also allows both motors to be placed in the vicinity of the body, thereby minimizing leg inertia.

The utilization of two four-bar mechanisms and a timing belt system classifies the RML as a *single-DOF coupled serial chain mechanism* that takes advantage of the mechanical constraints between articulations to guide end effector (foot) motions [31].

Although planar feet perform well on flat terrain, the foot should be capable of traversing uneven terrain as well. A passive suspension system, inspired by the active locking foot mechanism in Ref. [32], is integrated into the foot that permits vertical translation of four toes. Compression springs between the foot and each toe provide compliance that softens impact and maintains a stable support polygon with four points of contact, even in the presence of uneven terrain. Shock absorbent gel pads are placed at the end of each toe to further improve compliance and contact surface area. A linear pattern of retaining ring groves is incorporated into the toes to allow modification of each spring's precompression.

Linear potentiometers measure the displacement of each toe. Knowing the spring's stiffness, this sensory feedback can be used to determine the foot's contact forces with the ground and calculate the zero moment point stability criteria of the legged robot [33]. The passive suspension system enables the RML to walk on uneven terrain.

Design symmetry of the structural components of the RML enables the construction of multilegged robots by interconnecting similar modules via its connector ports (Fig. 1). For example, a quadruped configuration consisting of four RMLs has been presented in Ref. [22].

3   System Model

This section presents the mathematical models for the kinematics (Sec. 3.1) and dynamics (Sec. 3.2) of the RML.

3.1   Single-Leg Kinematics. The parallelogram structure of the RML discussed in Sec. 2 allows for simplification of the
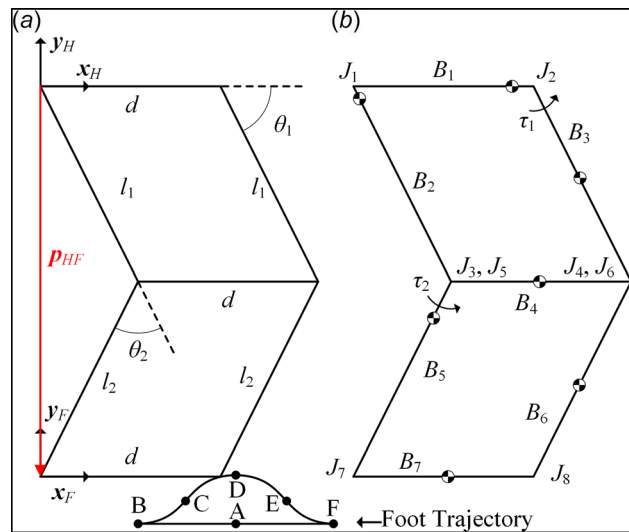

Fig. 2   Single-leg model: (*a*) kinematic variables and (*b*) dynamic variables

single-leg kinematics model into a planar elbow manipulator [34]. The leg schematic shown in Fig. 2(*a*) defines the kinematic model parameters, including the hip length l_1, shin length l_2, and the position vector from the hip frame to the foot frame $\boldsymbol{p}_{\mathrm{HF}}$. The forward kinematics of the leg are defined in Eq. (1) with respect to the hip frame coordinate system, where s_1 and c_1 denote the sine and cosine of θ_1 and s_{12} and c_{12} denote the sine and cosine of $\theta_1 + \theta_2$. Given the planar topology of the leg, the y-coordinates of each body remain constant

$$\begin{cases} l_1 c_1 + l_2 c_{12} = p_{\mathrm{HF},x} \\ -l_1 s_1 - l_2 s_{12} = p_{\mathrm{HF},z} \end{cases} \qquad (1)$$

For a prescribed $\boldsymbol{p}_{\mathrm{HF}}$ in the leg workspace, the leg's inverse kinematics are analytically calculable; within the workspace boundaries, two solutions can be found for a given $\boldsymbol{p}_{\mathrm{HF}}$ (knee forward and knee behind), and on the workspace boundaries, one solution can be found.

The forward velocity kinematics are found by differentiating Eq. (1), as shown in Eq. (2). Joint angle velocities are calculable from the prescribed $\dot{\boldsymbol{p}}_{\mathrm{HF}}$, when $\sin \theta_2$ (the Jacobian determinant) is not equal to zero

$$\begin{bmatrix} -l_1(s_1 + s_{12}) & -l_1 s_{12} \\ -l_2(c_1 + c_{12}) & -l_2 c_{12} \end{bmatrix} \begin{bmatrix} \dot{\theta}_1 \\ \dot{\theta}_2 \end{bmatrix} = \begin{bmatrix} \dot{p}_{\mathrm{HF},x} \\ \dot{p}_{\mathrm{HF},z} \end{bmatrix} \qquad (2)$$

3.2   Single-Leg Dynamics. Unlike the single-leg kinematics, the single-leg dynamics cannot be generalized by a serial robotic structure; a model representing the double-four-bar structure is needed to extract the joint requirements to drive the thigh and shin linkages given the gravitational loading on each link, as well as the external loading applied on the leg from the hip/foot.

Given the closed-loop kinematic structure of the thigh and shin, spatial generalized coordinates are used to calculate the leg dynamics [35]. For each of the seven bodies shown in Fig. 2(*b*) labeled as B_{1-7}, seven coordinates are defined—three Cartesian coordinates and four Euler parameters—which create a joint space of 49 variables. Forty-nine constraint equations are required to ensure this model is well posed; the constraints utilized are described in Table 1.

The fixed constraint rigidly connects either the hip (B_1) or foot (B_7) to ground and does not allow for relative linear or angular displacement.

Table 1 Dynamic model constraints

Constraint	Qty.	Eqs. per constraint	Total
Fixed	1	6	6
Revolute-5	6	5	30
Revolute-2	2	2	4
Angle driver	2	1	2
Normality	7	1	7
Number of constraint equations			49

The revolute joint constraints, located at joints J_{1-8} as shown in Fig. 2(b), prescribe two points on two bodies to coincide and allow relative rotation about a shared axis. Because the linkages are topologically planar (i.e., the four revolute joint axes in each four-bar are parallel), for each parallelogram, one of the four revolute joints must be reduced DOF to avoid overconstraining the model—after specifying the three five-equation revolute joints, only the x- and y-coordinates of the final joint need to be prescribed as coinciding, hence the two-equation revolute joint constraints.

The angle driver constraint prescribes the relative angle between two bodies connected by a revolute joint.

The normality constraint ensures that the norm of each body's set of four Euler parameters remains one, allowing these four coordinates to represent a generalized spatial rotation.

Equation (3) defines the dynamic model in terms of the 21 Cartesian coordinate accelerations $\ddot{p}$, the 28 Euler parameter accelerations $\ddot{e}$, and the 49 Lagrange multipliers λ, where $\mathbf{M}$ is a block diagonal matrix of the link mass tensors, $\mathbf{J}$ is a block diagonal matrix of the link inertia tensors, Φ_p and Φ_e are Jacobians of the constraint vector Φ with respect to the Cartesian coordinates (Φ_p) and Euler parameters (Φ_e), F and n are forcing functions associated with the external forces, external moments, and gyroscopic moments acting on each body, and γ are the acceleration-independent terms associated with twice differentiating the constraint vector Φ [35]

$$\begin{bmatrix} \mathbf{M} & 0 & \Phi_p^T \\ 0 & \mathbf{J} & \Phi_e^T \\ \Phi_p & \Phi_e & 0 \end{bmatrix} \begin{bmatrix} \ddot{p} \\ \ddot{e} \\ \lambda \end{bmatrix} = \begin{bmatrix} F \\ n \\ -\gamma \end{bmatrix} \tag{3}$$

The Lagrange multipliers λ correspond to the forces and moments required to maintain the various constraints. The Lagrange multipliers associated with the two angle driver constraints correspond to the torque required to actuate those joints. Other Lagrange multipliers may be utilized to estimate the force loading transmitted through various leg lengths.

4 Foot Trajectory Planning

Trajectory planning involves the process of generating foot trajectories in space relative to the hip coordinate frame. Figure 2(a) shows a single-cycle foot trajectory that consists of two main phases: the swing phase (B–F) and the support phase (F–A–B). The swing phase lifts the foot and advances it to the start of its next support phase, and the support phase generates the ground normal force to support the robot. A straight line support phase is desired to maintain a constant robot body height and minimize energy requirements during a walking gait [6].

Quintic polynomials are used to generate vertical foot position/velocity/acceleration trajectories. Boundary conditions include the start and end step heights, and zero velocity/acceleration at the start and end points. A linear equation was used to generate the trajectory for the straight line support phase. A vector of uniformly spaced horizontal position points (providing a constant horizontal foot velocity) was used with the vertical foot trajectory to control the swing phase [22]. Joint angle trajectories were then computed using the kinematic model in Sec. 3.1.

The generated foot trajectories have been demonstrated in producing a forward walking trot gait using multibody dynamic simulations of a quadruped configuration composed of four RMLs [22].

5 Experimental Results

In this section, results are presented that utilize the leg's dynamic model to analyze the motor actuation requirements (Sec. 5.1) and to experimentally validate the leg's kinematic model on an integrated prototype of the RML by studying its performance in tracking a foot trajectory (Sec. 5.2).

5.1 Estimating Actuation Requirements. After generating a preliminary design for the leg, the kinematics and dynamics models were used to analyze the speed and torque requirements to aid motor selection.

The kinematic and dynamic models presented may be utilized for two types of simulations: fixed-hip and fixed-foot. In the fixed-hip simulation, the body of the legged robot is assumed to be a fixed frame, with the foot lifting from the ground and moving with respect to the hip. In the fixed-foot simulation, the foot maintains contact with the ground while supporting the leg and any external force applied on the hip by the other components of the legged robot.

For the motor speed analysis (kinematic), the results from these two models are equivalent and may be mapped into one another by a kinematic transformation. However, for the torque analysis (dynamic), the fixed-hip and fixed-foot models represent distinct modes of operation for the leg (swing versus support phases). Due to the need for the leg to support some of the weight of the legged robot during the support phase, the fixed-foot model will be used in this analysis to determine the maximum motor torque requirements.

After generating a preliminary design for the RML, the mass and geometric properties of this design were extracted using CAD software. The relevant properties used in these simulations are summarized in Tables 2 and 3. With reference to Fig. 2(b), the center-of-mass coordinates for each body are defined in a body-frame coordinate system centered at joint i with its x-axis defined along the unit vector from joint i (J_i) to joint j (J_j), the z-axis coming out of the page, and the associated y-axis completing the right-handed coordinate system.

The foot trajectory described in Sec. 4 maintains a constant distance between the hip and foot joints during the straight line support phase. This is analogous to holding the hip trajectory at a constant height $p_{\mathrm{FH},y} = -p_{\mathrm{HF},y} = 330\,\mathrm{mm}$ relative to the foot joints. In addition, the foot trajectory in Sec. 4 moves along a prescribed step length distance during its support phase. For a step length of 150 mm centered with respect to the foot and

Table 2 RML geometric properties

Property	Value	Property	Value
d	120.1 mm	l_1, l_2	180 mm

Table 3 RML mass properties

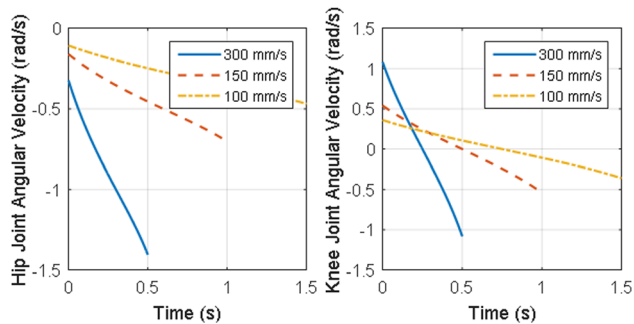| Body	J_i	J_j	Mass (kg)	z-axis inertia (kg m^2)	Center-of-mass (mm)
B_1	J_1	J_2	1.708	0.0132	[109.26, 0, 0]
B_2	J_1	J_3	1.645	0.0081	[−4.64, −11.57, 0]
B_3	J_2	J_4	0.145	0.0009	[102.73, 0, 0]
B_4	J_3	J_4	0.108	0.0004	[56.83, 0, 0]
B_5	J_5	J_7	0.382	0.0020	[39.43, 0, 0]
B_6	J_6	J_8	0.171	0.0011	[90, 0, 0]
B_7	J_7	J_8	0.509	0.0031	[60.15, −31.97, 0]

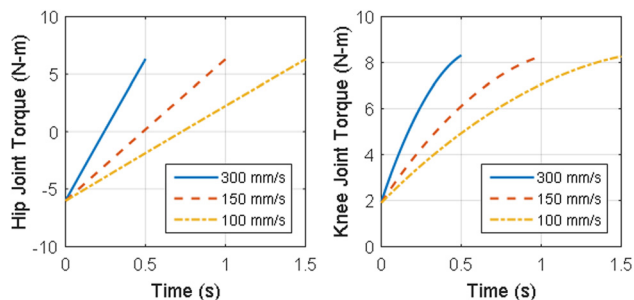**Fig. 3 Motor speed analysis for varying hip speeds**

Fig. 4 Motor torque analysis for varying hip speeds

hip, the hip will move from 75 mm behind the hip joint ($p_{FH,x} = -p_{HF,x} = -75$ mm) to 75 mm before the hip joint ($p_{FH,x} = -p_{HF,x} = 75$ mm) over a prescribed time period τ at a constant hip velocity speed of $150/\tau$ mm/s.

To mimic the additional loading from the legged robot during the support phase, an external force representing a second leg opposite the leg under consideration is applied to the hip link. This force is the gravitational force due to the total mass of the leg (4.668 kg) applied at the center-of-mass position with respect to

the hip-fixed frame ([55.71, −71.60, 0] mm) when each hip joint is directly above its respective foot joint (i.e., when $p_{FH,x} = 0$ mm and $p_{FH,y} = 330$ mm).

Figures 3 and 4 show the motor speeds and motor torques, respectively, required for support phases traversing the 150 mm step length in $\tau = \{0.5, 1.0, 1.5\}$ s. The required joint velocity increases nonlinearly as the hip velocity increases, yet the required joint torques maintain similar profiles with different time scaling. This is due to the fact that the external loading acting on the leg does not vary with time. As a result, the mapping of this loading into the joint torques depends only on the instantaneous geometry of the leg at a given time and not the speed at which that geometry changes.

The knee angular velocity, shown in Fig. 3, changes sign due to the thigh link passing through a vertical configuration in relation to the foot, causing the shin to initially rotate toward the foot in the $+z$ direction, then away from it, as the constant hip height relative to the foot is maintained. In Fig. 4, the knee torque is positive throughout each simulation to oppose the links' gravitational loading and the hip's external loading from "collapsing" the knee. This torque changes over time despite the constant external loading on each rigid body due to the torque's dependence on the leg configuration.

The servomotors selected to actuate the hip and knee joints provide a maximum of 11.3 N m of torque and 120 deg/s (2.09 rad/s) angular velocity. The estimated motor requirements fall within the motor specifications, with margins of 2.98 N m and 0.68 rad/s for the motor torque and speed, respectively.

5.2 Leg Prototype Experiments. Structural components were fabricated with acrylonitrile butadiene styrene thermoplastic using a 3D printer. The RML prototype's weight is 4.7 kg and measures 368 mm in a fully extended configuration.

A Teensy 3.1 MCU was connected to a computer via a universal serial bus-serial port and used to send joint trajectories to the servomotors. To ensure stable response of servomotors, the joint trajectories were sampled at an update rate of 50 Hz using linear interpolation.

A series of experiments were conducted to measure the accuracy and repeatability of the RML in tracking a desired foot
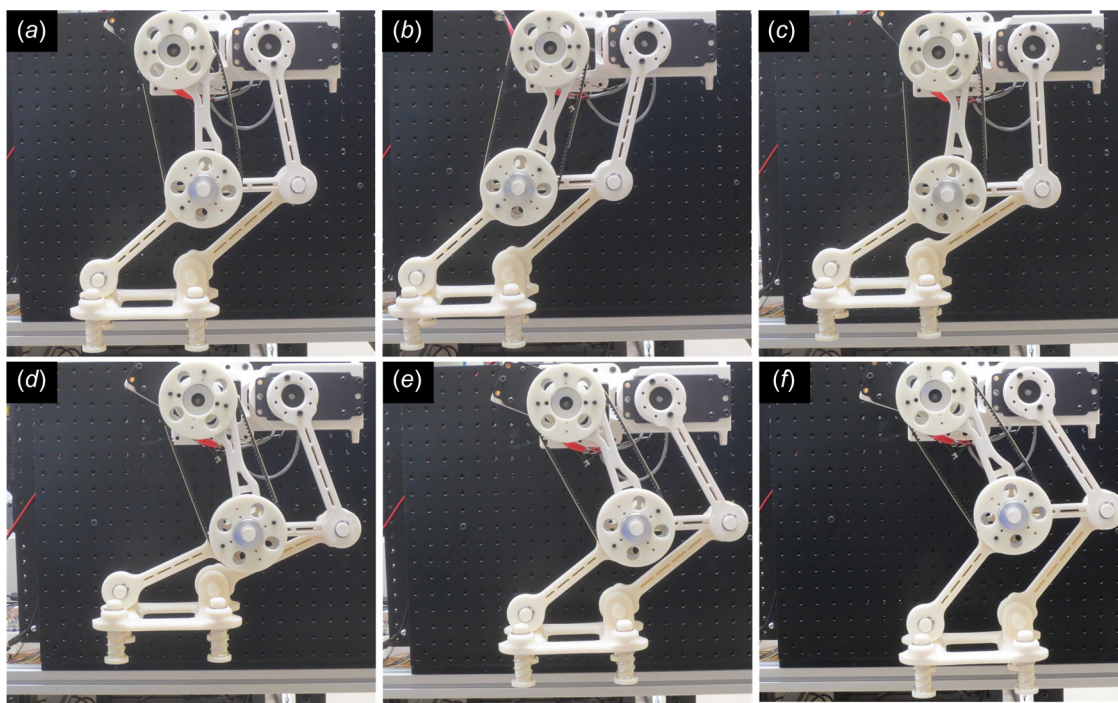

Fig. 5 Integrated RML prototype tracking a foot trajectory at key points A, B, C, D, E, and F
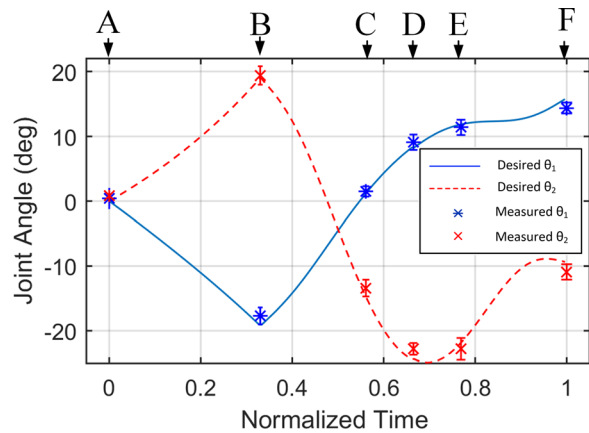
Fig. 6 Measured results of joint angle mean and standard deviation at the key points compared with desired joint trajectories

trajectory. Analyzing these parameters is critical to measure the mechanism's effectiveness in reproducing a variety of walking gaits, since deviations from desired trajectories may cause undesirable effects. For example, large tracking errors during the support phase may create impulsive forces or swaying of the legged robot body that causes loss of stability and tipping over.

To test the mechanisms accuracy and repeatability, the RML prototype was rigidly grounded to a wall via its connector ports as shown in Fig. 5 and programed to track ten cycles of a foot trajectory in midair, in both clockwise and counterclockwise directions, with a step height of 50 mm and a step length of 150 mm. A tracking camera was mounted orthogonally to the RML to capture joint angles at key points A, B, C, D, E, and F (Fig. 2(a)) during the foot trajectory. This data was then used to compute the mean and standard deviation of measured joint angles. Measured data were then compared with the desired joint angles computed from inverse kinematics.

Initial experimental results indicated that the RML had two main sources of tracking error: (1) angular offsets at the home configuration measuring $\Delta\theta_1 = 1$ deg and $\Delta\theta_2 = 6$ deg and (2) a bidirectional timing belt backlash that caused θ_2 to lead the desired trajectory by 2 deg in the positive direction and lag by -2 deg in the negative direction. These sources of error were compensated for by calibrating the servomotor home configuration and providing additional angular rotations to account for the bidirectional lead and lag.

The experiments were then repeated after calibration and input compensation. Figure 6 presents measured results of joint angle mean and standard deviation at the key points compared with desired joint trajectories. Results indicate that θ_1 and θ_2 demonstrated an average angular error equivalent to 0.6 deg and 1.2 deg, respectively, and repeatability in the range of ±1.1 deg. A maximum deviation from the straight line support phase was recorded to be 5.2 mm, a significant improvement from the 20 mm deviations reported in Ref. [22].

6 Conclusion

This paper presented the design of a reduced-DOF RML mechanism that utilizes two serially connected four-bar mechanisms and a timing belt system to guide the motion of a flat foot. Kinematic and dynamic models were developed to analyze actuation requirements for the leg and aid motor selection. Experimental results were used to improve the accuracy and repeatability of the mechanism that demonstrated satisfactory performance in tracking a foot trajectory. The RML prototype exhibited a maximum angular error of 0.6 deg and 1.2 deg, for θ_1 and θ_2, respectively, and repeatability of ±1.1 deg. These results correspond to a maximum deviation from the straight line support phase equivalent to 5.2 mm.

Future work will involve the redesign of structural components for metal manufacturing to improve strength and accuracy. In addition, the servomotors will be replaced with high-performance geared DC motors with position and velocity feedback to achieve more accurate tracking of foot trajectories. Methods to replace the timing belt system to eliminate backlash will be investigated to enhance the mechanism's accuracy and repeatability and provide the desired straight line support phase. Sensitivity analysis will be investigated to optimize the relative dimensions of the leg (e.g., hip and shin lengths and coupler spacing) for a desired step length to minimize the required motor speeds and torques. The RML will be used to construct a quadruped and biped configuration to provide stable experimental platforms to study the performance advantages that attached robotic tail can provide to legged robots in terms of stabilization and maneuverability.

References

[1] Silva, M. F., and Machado, J. T., 2007, "A Historical Perspective of Legged Robots," J. Vib. Control, **13**(9–10), pp. 1447–1486.
[2] Song, S.-M., and Waldron, K. J., 1989, *Machines That Walk: The Adaptive Suspension Vehicle*, MIT Press, Cambridge, MA.
[3] Arikawa, K., and Hirose, S., 2007, "Mechanical Design of Walking Machines," Philos. Trans. R. Soc. A, **365**(1850), pp. 171–183.
[4] Galvez, J. A., Estremera, J., and De Santos, P. G., 2003, "A New Legged-Robot Configuration for Research in Force Distribution," Mechatronics, **13**(8), pp. 907–932.
[5] Chen, X., Wang, L.-Q., Ye, X.-F., Wang, G., and Wang, H.-L., 2013, "Prototype Development and Gait Planning of Biologically Inspired Multi-Legged Crablike Robot," Mechatronics, **23**(4), pp. 429–444.
[6] Kaneko, M., Abe, M., Tachi, S., Nishizawa, S., Tanie, K., and Komoriya, K., 1985, "Legged Locomotion Machine Based on the Consideration of Degrees of Freedom," *Theory and Practice of Robots and Manipulators*, Springer, New York, pp. 403–410.
[7] Tang, Y., Ma, S., Sun, Y., and Ge, D., 2012, "A Multi-Legged Robot With Less Actuators by Applying Passive Body Segment Joint," Intelligent Robots and Systems (IEEE), Vilamoura, Portugal, Oct. 7–12, pp. 1828–2833.
[8] Schwab, A., and Wisse, M., 2001, "Basin of Attraction of the Simplest Walking Model," ASME Paper No. DETC2001/VIB-21363.
[9] Torige, A., Noguchi, M., and Ishizawa, N., 1993, "Centipede Type Multi-Legged Walking Robot," Intelligent Robots and Systems (IEEE), Tokyo, Japan, July 26–30, pp. 567–571.
[10] Hoffman, K. L., and Wood, R. J., 2011, "Passive Undulatory Gaits Enhance Walking in a Myriapod Millirobot," IEEE/RSJ International Conference on Intelligent Robots and Systems, San Francisco, CA, Sept. 25–30, pp. 1479–1486.
[11] Saranli, U., Buehler, M., and Koditschek, D. E., 2001, "Rhex: A Simple and Highly Mobile Hexapod Robot," Int. J. Rob. Res., **20**(7), pp. 616–631.
[12] Jimenez, B., and Ikspeert, A., 2007, "Centipede Robot Locomotion," Master's thesis, Ecole Polytechnique Federale de Lausanne, Lausanne, Switzerland.
[13] Yoneda, K., Ota, Y., Ito, F., and Hirose, S., 2000, "Construction of a Quadruped With Reduced Degrees of Freedom," Industrial Electronics Society (IEEE), Nagoya, Japan, Oct. 22–28, pp. 28–33.
[14] Funabashi, H., Ogawa, K., Gotoh, Y., and Kojima, F., 1985, "Synthesis of Leg-Mechanisms of Biped Walking Machines—Part I: Synthesis of Ankle Path Generator," Bull. JSME, **28**(237), pp. 537–543.
[15] Kaneko, M., Abe, M., Tanie, K., Tachi, S., and Nishizawa, S., 1985, "Basic Experiments on a Hexapod Walking Machine (MELWALK III) With an Approximate Straight-Line Link Mechanism," International Conference on Advanced Robotics (IEEE), St. Louis, MO, pp. 397–410.
[16] Liang, C., Ceccarelli, M., and Takeda, Y., 2008, "Operation Analysis of a One-DOF Pantograph Leg Mechanisms," 17th International Workshop on Robotics in Alpe-Adria-Danube Region (IEEE), Ancona, Italy, Sept. 15–17, pp. 15–17.
[17] Lokhande, N., and Emche, V., 2013, "Mechanical Spider by Using Klann Mechanism," Int. J. Mech. Eng. Comput. Appl., **1**(5), pp. 13–16.
[18] Tavolieri, C., Ottaviano, E., Ceccarelli, M., and Rienzo, A., 2006, "Analysis and Design of a 1-DOF Leg for Walking Machines," 15th International Workshop on Robotics in Alpe-Adria-Danube Region (IEEE), Balatonfured, Hungary, pp. 15–17.
[19] Adachi, H., Koyachi, N., and Nakano, E., 1988, "Mechanism and Control of a Quadruped Walking Robot," IEEE Control Syst. Mag., **8**(5), pp. 14–19.
[20] Lovasz, E. C., Pop, C., Pop, F., and Dolga, V., 2014, "Novel Solution for Leg Motion With 5-Link Belt Mechanism," Int. J. Appl. Mech. Eng., **19**(4), pp. 699–708.

[21] Collins, S., Ruina, A., Tedrake, R., and Wisse, M., 2005, "Efficient Bipedal Robots Based on Passive-Dynamic Walkers," Science, **307**(5712), pp. 1082–1085.

[22] Saab, W., and Ben-Tzvi, P., 2016, "Design and Analysis of a Robotic Modular Leg," ASME Paper No. DETC2016-59388.

[23] Rone, W. S., and Ben-Tzvi, P., 2012, "Continuum Manipulator Statics Based on the Principle of Virtual Work," ASME Paper No. IMECE2012-87675.

[24] Rone, W. S., and Ben-Tzvi, P., 2013, "Multi-Segment Continuum Robot Shape Estimation Using Passive Cable Displacement," IEEE International Symposium on Robotic and Sensors Environments, Washington, DC, Oct. 21–23, pp. 37–42.

[25] Rone, W. S., and Ben-Tzvi, P., 2014, "Continuum Robotic Tail Loading Analysis for Mobile Robot Stabilization and Maneuvering," ASME Paper No. DETC2014-34678.

[26] Rone, W. S., and Ben-Tzvi, P., 2014, "Mechanics Modeling of Multisegment Rod-Driven Continuum Robots," ASME J. Mech. Rob., **6**(4), p. 041006.

[27] Rone, W. S., and Ben-Tzvi, P., 2014, "Continuum Robot Dynamics Utilizing the Principle of Virtual Power," IEEE Trans. Rob., **30**(1), pp. 275–287.

[28] Rone, W. S., and Ben-Tzvi, P., 2015, "Static Modeling of a Multi-Segment Serpentine Robotic Tail," ASME Paper No. DETC2015-46655.

[29] Rone, W. S., and Ben-Tzvi, P., 2016, "Dynamic Modeling and Simulation of a Yaw-Angle Quadruped Maneuvering With a Planar Robotic Tail," ASME J. Dyn. Syst. Meas. Control, **138**(8), p. 084502.

[30] Saab, W., and Ben-Tzvi, P., 2016, "Design and Analysis of a Discrete Modular Serpentine Tail," ASME Paper No. DETC2016-59387.

[31] Krovi, V., Ananthasuresh, G., and Kumar, V., 2002, "Kinematic and Kineto-static Synthesis of Planar Coupled Serial Chain Mechanisms," ASME J. Mech. Des., **124**(2), pp. 301–312.

[32] Hashimoto, K., Hosobata, T., Sugahara, Y., Mikuriya, Y., Sunazuka, H., Kawase, M., Lim, H.-O., and Takanishi, A., 2005, "Development of Foot System of Biped Walking Robot Capable of Maintaining Four-Point Contact," IEEE/RSJ International Conference on Intelligent Robots and Systems, Calgary, AB, Canada, Aug. 2–6, pp. 1361–1366.

[33] Vukobratović, M., and Borovac, B., 2004, "Zero-Moment Point—Thirty Five Years of Its Life," Int. J. Humanoid Rob., **1**(1), pp. 157–173.

[34] Spong, M. W., Hutchinson, S., and Vidyasagar, M., 2006, *Robot Modeling and Control*, Wiley, New York.

[35] Haug, E. J., 1989, *Computer Aided Kinematics and Dynamics of Mechanical Systems*, Allyn and Bacon, Boston, MA.